### Title
Understanding How Wnt Influences Destruction Complex Activity and β-Catenin Dynamics




### Authors
Mukherjee, Abhirup
Dhar, Neha
Stathos, Mark
et al.



### Publication Date
2018-08-01

### DOI
10.1016/j.isci.2018.07.007

Peer reviewed

iScience

CellPress

Article

# Understanding How Wnt Influences Destruction Complex Activity and β-Catenin Dynamics

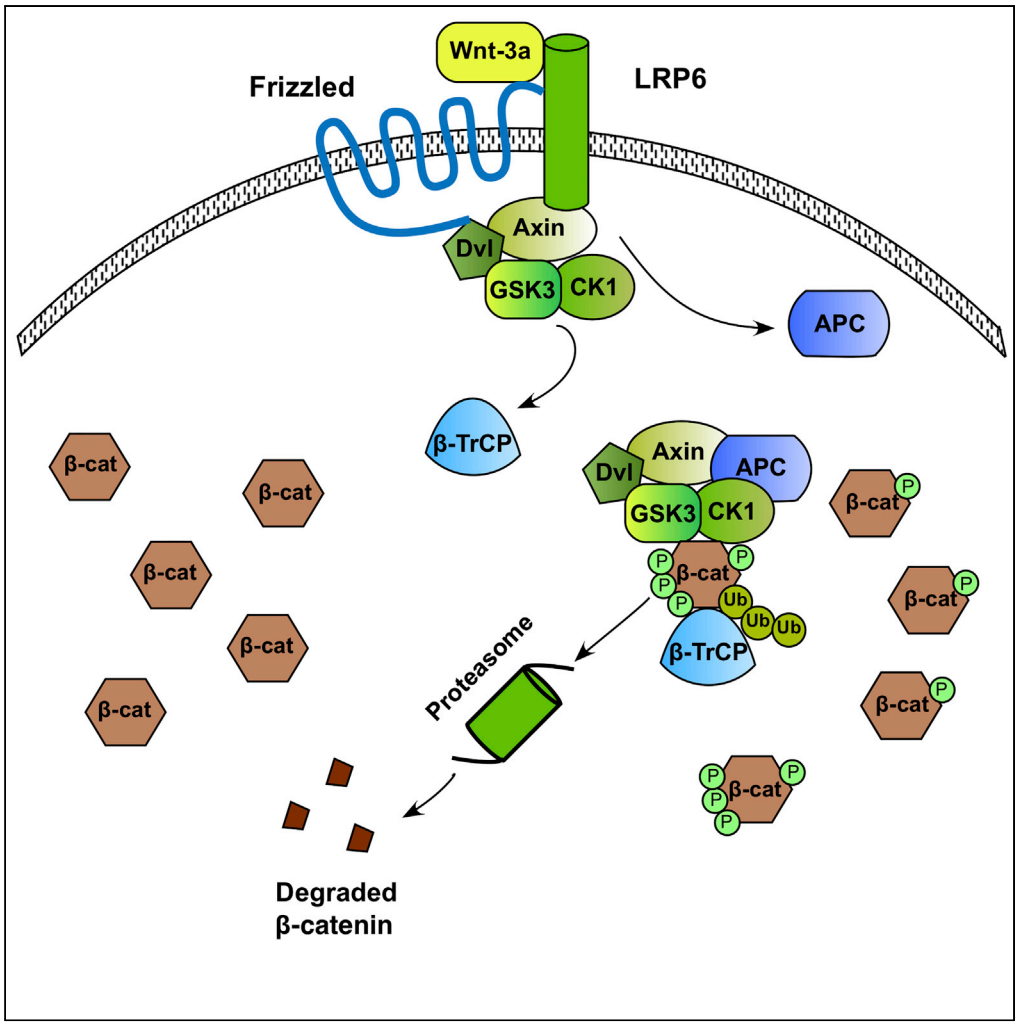


Abhirup Mukherjee, Neha Dhar, Mark Stathos, David V. Schaffer, Ravi S. Kane

schaffer@berkeley.edu (D.V.S.)
ravi.kane@chbe.gatech.edu (R.S.K.)

## HIGHLIGHTS

Wnt signaling partially inhibits both β-catenin phosphorylation and ubiquitination

Some destruction complexes relocalize to the cellular membrane upon Wnt stimulation

Analysis supports a distributive mechanism for destruction complex activity

Mukherjee et al., iScience 6, 13–21
August 31, 2018 
https://doi.org/10.1016/j.isci.2018.07.007

iScience

CellPress

Article

# Understanding How Wnt Influences Destruction Complex Activity and β-Catenin Dynamics

Abhirup Mukherjee,[1] Neha Dhar,[1] Mark Stathos,[1] David V. Schaffer,[2,3,4,*] and Ravi S. Kane[1,5,*]

## SUMMARY

**Despite extensive research on the canonical Wnt signaling pathway, the mechanism by which this signal downregulates the activity of destruction complexes and inhibits β-catenin degradation remains controversial. In particular, recent attention has focused on two main competing mechanisms—inhibition of phosphorylation and inhibition of ubiquitination. Our combined experimental and theoretical analysis demonstrates that the disassembly of a fraction of the intracellular destruction complexes results in the partial inhibition of *both β-catenin phosphorylation and ubiquitination*. This inhibition is spatially patterned, consistent with the relocalization of some destruction complexes to the cellular membrane upon Wnt stimulation. Moreover, in contrast to the generally accepted view that the destruction complex is highly processive, our analysis supports a distributive model, in which β-catenin can dissociate from the complex between sequential phosphorylation events. Understanding the fundamental mechanism by which Wnt signaling is regulated provides a rational basis for tuning the pathway for scientific and therapeutic purposes.**

## INTRODUCTION

The canonical Wnt signaling pathway has been the subject of extensive research given its fundamental role in biological processes ranging from development to controlling stem cell fate and because of the association of abnormal Wnt signaling with cancers (Azzolin et al., 2014; Bilic et al., 2007; Clevers, 2006; Cong et al., 2004; Hernandez et al., 2012; Kim et al., 2013; Li et al., 2012; Nelson and Nusse, 2004; Nusse and Clevers, 2017; Nusse and Varmus, 2012; Peifer and Polakis, 2000). In the absence of a Wnt signal, β-catenin binds to the destruction complex and is sequentially phosphorylated by CK1 (at Ser45) and GSK3 (at Ser33/37/Thr41), then ubiquitinated by the β-TrCP ubiquitin E3 ligase complex, and finally degraded by the proteasome (Nusse and Clevers, 2017). The continuous synthesis and degradation of β-catenin collectively result in a low steady-state level of this Wnt effector (Hernandez et al., 2012). The canonical Wnt signaling pathway is activated by the binding of Wnt to its cellular receptors Frizzled (Fzd) and LRP5/6 (Cong et al., 2004; Nusse and Clevers, 2017). Wnt stimulation inhibits the destruction complex-mediated degradation of β-catenin by a mechanism that remains controversial, but results in an increase in the cytosolic concentration of β-catenin. The accumulated β-catenin translocates to the nucleus and, together with the T-cell factor (TCF) family of transcription factors, activates transcription (Cong et al., 2004).

Although numerous mechanisms have been proposed to explain the Wnt-mediated increase in levels of β-catenin, recent attention has focused on two main competing mechanisms—inhibition of ubiquitination and inhibition of phosphorylation (Figure 1A) (Azzolin et al., 2014; Hernandez et al., 2012; Kim et al., 2013; Li et al., 2012). Li et al. (2012) observed that the cytosolic accumulation of β-catenin was detectable as early as 30 min following Wnt treatment. They concluded that this initial activation of the Wnt pathway could not be caused by Axin1 degradation, since significant degradation of Axin1 was not observed until 4 hr post-Wnt stimulation (Li et al., 2012). To elucidate the mechanism of Wnt activation, Li et al. (2012) immunoprecipitated Axin1 and thus pulled down the other proteins associated with the destruction complex. Their experiments suggested that the destruction complex remained intact following Wnt stimulation. They reported that the concentrations of CK1-phosphorylated β-catenin (CK1-p-β-cat) and GSK3-phosphorylated β-catenin (GSK3-p-β-cat) associated with Axin1 increased, whereas the amount of ubiquitinated GSK3-p-β-cat associated with Axin1 decreased after Wnt stimulation. Li et al. (2012) concluded that Wnt stimulation led to a temporary inactivation-by-saturation of the destruction complex with GSK3-p-β-cat. Azzolin et al. (2014) also suggested a primary role for the inhibition of ubiquitination. They reported that the Hippo transducer proteins YAP/TAZ formed a part of the destruction complex and

[1]School of Chemical & Biomolecular Engineering, Georgia Institute of Technology, Atlanta, GA 30332, USA

[2]Department of Chemical Engineering, University of California Berkeley, Berkeley, CA 94720, USA

[3]Department of Bioengineering, University of California, Berkeley, Berkeley, CA 94720, USA

[4]Helen Wills Neuroscience Institute, University of California, Berkeley, Berkeley, CA 94720, USA

[5]Lead Contact

*Correspondence: schaffer@berkeley.edu (D.V.S.), ravi.kane@chbe.gatech.edu (R.S.K.)

https://doi.org/10.1016/j.isci.2018.07.007

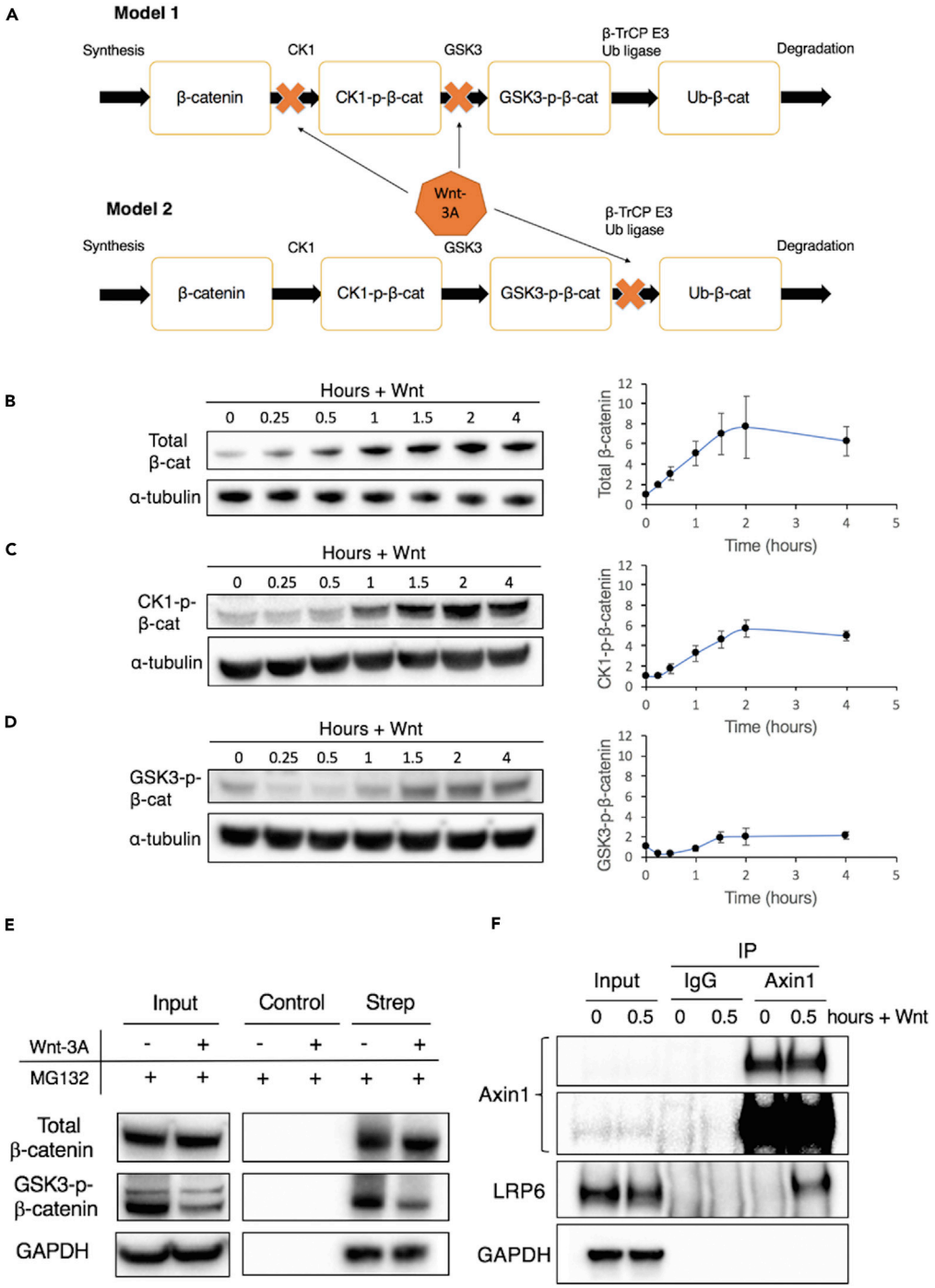


**Figure 1. Characterizing β-Catenin Dynamics in Response to Wnt-3A Stimulation**

(A) Schematic showing two models that have been proposed to explain Wnt-induced increases in levels of β-catenin. Model 1 (top) suggests that the inhibition of phosphorylation by CK1 and/or GSK3 causes β-catenin to accumulate in the cell, whereas Model 2 (bottom) is based on the inhibition of ubiquitination.

(B–D) Characterization of changes in the concentration of (B) non-membrane-associated β-catenin, (C) whole-cell CK1-phosphorylated-β-catenin, and (D) GSK3-phosphorylated-β-catenin with time upon Wnt stimulation through immunoblotting. Plots show mean ±1 SD (n = 3 replicates).

(E) Characterization of concentrations of newly synthesized azidohomoalanine-tagged proteins before (–) and after (+) Wnt stimulation after pull down with streptavidin-agarose beads (Strep) or agarose beads (control). Input lanes

**Figure 1. *Continued***
correspond to samples before pull down with streptavidin-agarose beads and therefore represent total protein, not newly synthesized AHA-tagged proteins. The input lanes were imaged separately.
(F) Characterization of changes in protein-protein interactions upon Wnt stimulation via co-immunoprecipitation (IP) using an anti-Axin1 antibody.
See also Figure S1.

were essential for the docking of the β-TrCP ubiquitin E3 ligase. They suggested that Wnt stimulation caused YAP/TAZ to be released from the destruction complex, preventing the docking of the E3 ligase and thus inhibiting ubiquitination.

In contrast, Hernandez et al. (2012) suggested a primary role for the inhibition of the CK1 and GSK3 phosphorylation steps. They stimulated mammalian cells with Wnt-3a and measured time-dependent changes in the concentrations of total and phosphorylated β-catenin. The total cytosolic β-catenin concentration initially increased with time and then reached a higher steady-state level, whereas the concentration of GSK3-p-β-cat decreased initially but subsequently recovered. Moreover, the maximum in the rate of accumulation of total β-catenin coincided in time with the minimum in the concentration of GSK3-p-β-cat. Kim et al. (2013) also reported that the ratio of the concentration of GSK3-p-β-cat to that of total β-catenin decreased significantly upon Wnt stimulation and never recovered over time and suggested that this decrease indicated a key role for the inhibition of phosphorylation. Hernandez et al. (2012) reasoned that these dynamics were inconsistent with inhibition at a step downstream of phosphorylation (e.g., ubiquitination) and also noted that their results were consistent with the inhibition of phosphorylation due to the disassembly of the destruction complex. Moreover, they argued that if Wnt caused complete inhibition of destruction complex activity by its saturation, then the degradation flux would not recover to its original level, resulting in an uncontrolled accumulation of β-catenin. Thus, a mechanistic model of Wnt signaling must also explain how β-catenin is maintained at an elevated steady-state level upon Wnt stimulation and what prevents it from accumulating indefinitely (Hernandez et al., 2012).

## RESULTS AND DISCUSSION

To clarify this issue, we conducted experiments using HEK293T cells, which have been used in many of the seminal mechanistic investigations of Wnt signaling (Azzolin et al., 2014; Hernandez et al., 2012; Kim et al., 2013; Li et al., 2012). We also stress that for the reasons noted by Li et al (Li et al., 2012), we did not use overexpression analyses and instead characterized endogenous destruction complexes.

We stimulated cultured HEK293T cells with Wnt-3a and first monitored changes in the levels of total β-catenin over time. A significant amount of β-catenin in these cells is reported to remain associated with membrane-bound E-cadherin complexes, a highly stable pool not involved in canonical Wnt signaling (Li et al., 2012). As a result, in keeping with prior studies, we removed the membrane-associated β-catenin fraction by incubating whole-cell lysates with concanavalin A-Sepharose 4B beads (Hernandez et al., 2012) and monitored changes in the level of free (cytoplasmic and nuclear) β-catenin over time (Figures 1B and S1). Consistent with the results of Hernandez et al. (2012), we observed that the concentration of total β-catenin increased 15 min after Wnt stimulation and reached an elevated steady-state concentration in approximately 2 hr (Figure 1B). Since the rate of synthesis of β-catenin does not change following Wnt stimulation (Hernandez et al., 2012), the observed accumulation of β-catenin suggests that its rate of degradation must initially decrease. However, 2 hr after Wnt stimulation, the rate of β-catenin degradation must recover to its original value to offset synthesis and thereby help maintain the new, elevated steady-state concentration of β-catenin. We also monitored changes in the levels of CK1-p-β-catenin in whole-cell lysates upon Wnt stimulation. Levels of CK1-p-β-catenin increased with time and also attained a higher steady-state value approximately 2 hr after Wnt stimulation (Figure 1C).

We next measured the changes in the levels of GSK3-p-β-cat in whole-cell lysates. We found that this level decreased initially upon Wnt stimulation and then recovered, reaching a steady state after 2 hr (Figure 1D). This observation is consistent with the inhibition of phosphorylation being responsible for the inhibition of β-catenin degradation, but is inconsistent with inhibition solely occurring downstream of phosphorylation (e.g., in the ubiquitination step). That is, as noted by Hernandez et al. (2012), if inhibition were to occur

downstream of phosphorylation, then GSK3-p-β-cat would continue to accumulate, which would in turn restore the degradation flux at a higher steady-state level of this species.

Next, we compared the GSK3 phosphorylation of newly synthesized β-catenin with and without Wnt stimulation using bioorthogonal noncanonical amino acid tagging (BONCAT) (Dieterich et al., 2007). In BONCAT, we tagged the newly synthesized proteins with L-azidohomoalanine, a non-canonical amino acid that contains an azide moiety. Using azide-alkyne "click" cycloaddition, the newly synthesized proteins can then be selectively labeled with biotin and pulled down using streptavidin beads (Debets et al., 2010). As seen in Figure 1E, newly synthesized β-catenin was GSK3-phosphorylated even after Wnt addition, indicating that some destruction complex activity was retained even after Wnt stimulation. The amount of newly synthesized GSK3-p-β-cat was, however, lower in the presence of Wnt than in its absence (Figure 1E), consistent with the partial inhibition of β-catenin phosphorylation upon Wnt stimulation. We next sought to understand the reason for this partial inhibition. It is well known that the binding of Wnt to its cellular receptors results in the relocalization of some destruction complexes to the cellular membrane (Bilic et al., 2007; Hendriksen et al., 2008; Li et al., 2012). Indeed, we immunoprecipitated Axin1 from whole-cell lysates and confirmed that LRP6 co-immunoprecipitated with Axin1 upon Wnt stimulation (Figure 1F). We hypothesized that the partial relocalization of destruction complexes to the cellular membrane may be responsible for the partial loss of destruction complex activity upon Wnt stimulation.

To further probe the mechanism of phosphorylation inhibition, we monitored changes in the levels of non-membrane-associated GSK3-p-β-cat and CK1-p-β-cat (i.e., the cytoplasmic and nuclear fraction) following Wnt stimulation (Figures 2A and S2). Importantly, the similarity in the levels of non-membrane-associated and whole-cell GSK3-p-β-cat at different time points after Wnt stimulation (Figure 2B) indicates that most of the GSK3-p-β-cat is *not* membrane associated. Similarly, the data in Figure 2B indicate that most CK1-p-β-cat is also not membrane associated. These results suggest that relocalization of destruction complexes to the membrane results in inhibition of their phosphorylation activity, with residual activity after Wnt stimulation primarily coming from non-membrane-associated destruction complexes.

Next, to probe the mechanism responsible for inhibition, we immunoprecipitated adenomatous polyposis coli (APC) and measured the changes in concentrations of Axin1 and GSK3-p-β-catenin being pulled down along with APC. We chose to immunoprecipitate APC in light of recent reports that APC levels are significantly lower than Axin1 levels in HEK293T cells (Kitazawa et al., 2017; Tan et al., 2012). We found that there was a significant decrease in Axin1-APC interactions upon Wnt stimulation, consistent with a partial disassembly of destruction complexes (Figures 2C and 2D). Valvezan et al. (2012) observed a similar decrease in Axin1-APC interactions in L cells upon Wnt stimulation. We also observed an initial decrease in the concentration of co-immunoprecipitated GSK3-p-β-cat (Figure 2C). These results indicate a partial disassembly of destruction complexes upon Wnt stimulation, resulting in an initial decrease in the rate of GSK3 phosphorylation and degradation of β-catenin. Levels of co-immunoprecipitated GSK3-p-β-cat had recovered substantially by 1.5 hr (Figure 2), consistent with β-catenin levels approaching a new steady state.

Collectively, the results from Figures 1 and 2 indicate that upon Wnt signaling, a fraction of the destruction complexes partitions to the membrane, which inhibits their activity and leads to the inhibition of β-catenin phosphorylation. The fraction of the destruction complexes in the cytosol, however, remains structurally intact and active. The decrease in the total number of active destruction complexes results in an initial decrease in the rate of β-catenin degradation and thus an increase in the intracellular concentration of β-catenin. Mass action then causes an increase in the rate of β-catenin phosphorylation by the remaining, active destruction complexes. At the new steady state following Wnt stimulation, the rate of degradation of β-catenin would once again equal its rate of synthesis, and the flux through the destruction complexes would be expected to return to its original value.

Figure 3A depicts the sequence of intracellular β-catenin modifications. The rate of phosphorylation by CK1 is governed by Michaelis-Menten kinetics, and for low substrate concentrations relative to the Michaelis constant ($K_{M1}$), it is given by $(k_{cat1}/K_{M1})[DC][B_0]$, where $k_{cat1}$ is the catalytic rate of CK1α on the destruction complex, [DC] is the destruction complex concentration, and $[B_0]$ is the concentration of unphosphorylated β-catenin (Hernandez et al., 2012). In Figure 3A, the rate constant $k_1=(k_{cat1}/K_{M1})[DC]$ (Hernandez et al., 2012). When [DC] decreases in response to Wnt stimulation, then an increase in $[B_0]$ would be required for the rate of CK1 phosphorylation, $(k_{cat1}/K_{M1})[DC][B_0]$, to recover (Figure 1B).

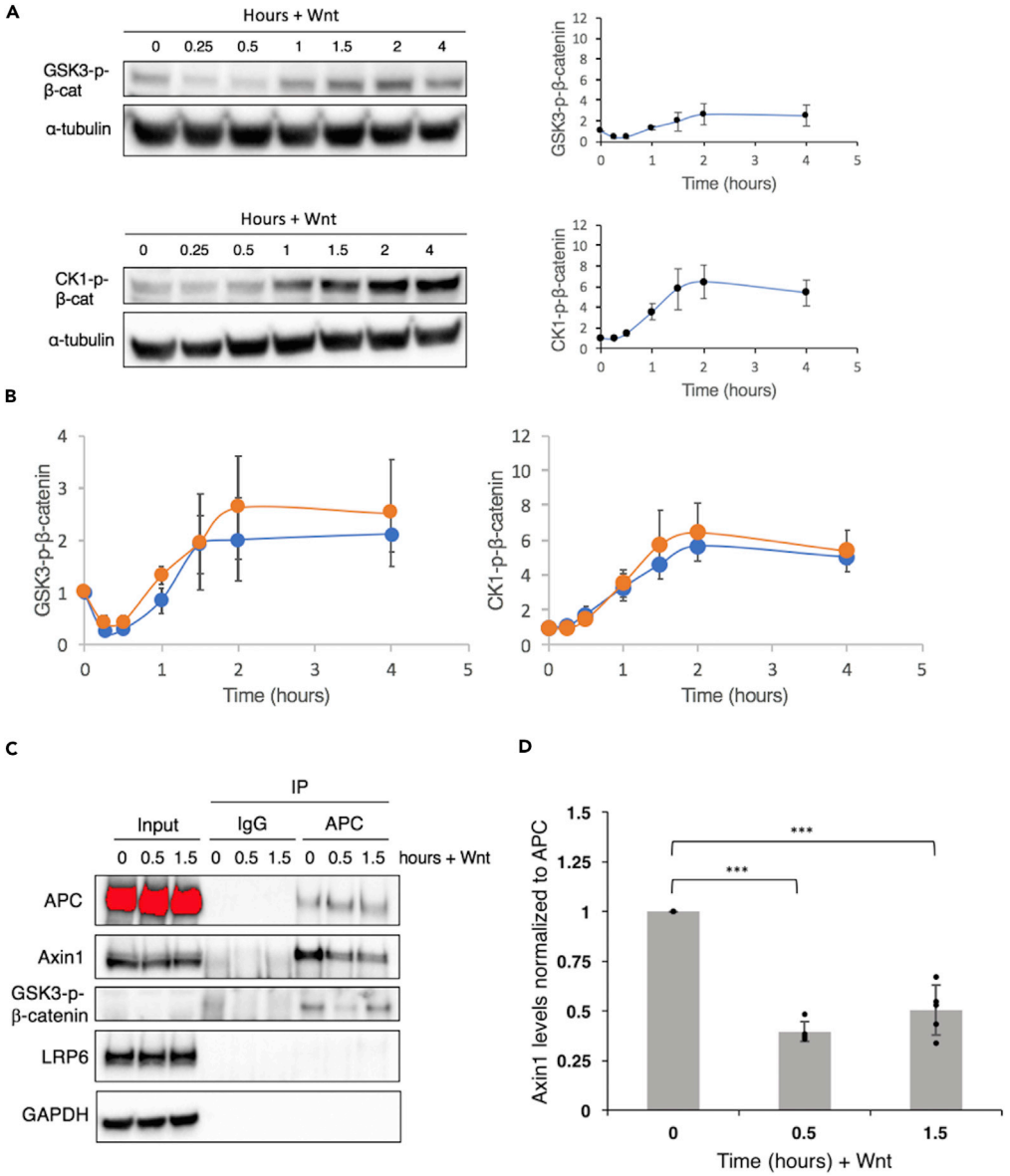


**Figure 2. Characterization of Destruction Complex Components upon Wnt Stimulation**

(A) Characterization of changes in concentration of non-membrane-associated GSK3-phosphorylated-β-catenin (top) and CK1-phosphorylated-β-catenin (bottom) with time upon Wnt stimulation through immunoblotting. Plots show mean ±1 SD (n = 3 replicates).

(B) Comparison of whole-cell (blue) and non-membrane associated (orange) concentrations of GSK3-phosphorylated-β-catenin (left) and CK1-phosphorylated-β-catenin (right). Plots show mean ±1 SD (n = 3 replicates).

(C) Monitoring changes in interactions of various proteins with APC upon Wnt signaling via co-immunoprecipitation (IP) using an anti-APC antibody.

(D) Quantifying changes in Axin1-APC interactions upon Wnt stimulation. Plot shows mean ±1 SD (n = 5 replicates), ***$p < 0.001$ by a two-tailed t test.

See also Figure S2.

We next used our results to analyze whether the destruction complex activity was processive or distributive. The generally accepted view is that the destruction complex is processive, with β-catenin undergoing a series of phosphorylations before being released from the complex. Our results—suggesting inhibition of phosphorylation due to partial disassembly that causes a decrease in the number of active destruction complexes—are inconsistent with this view. As explained by Hernandez et al. (2012), in the "processive"

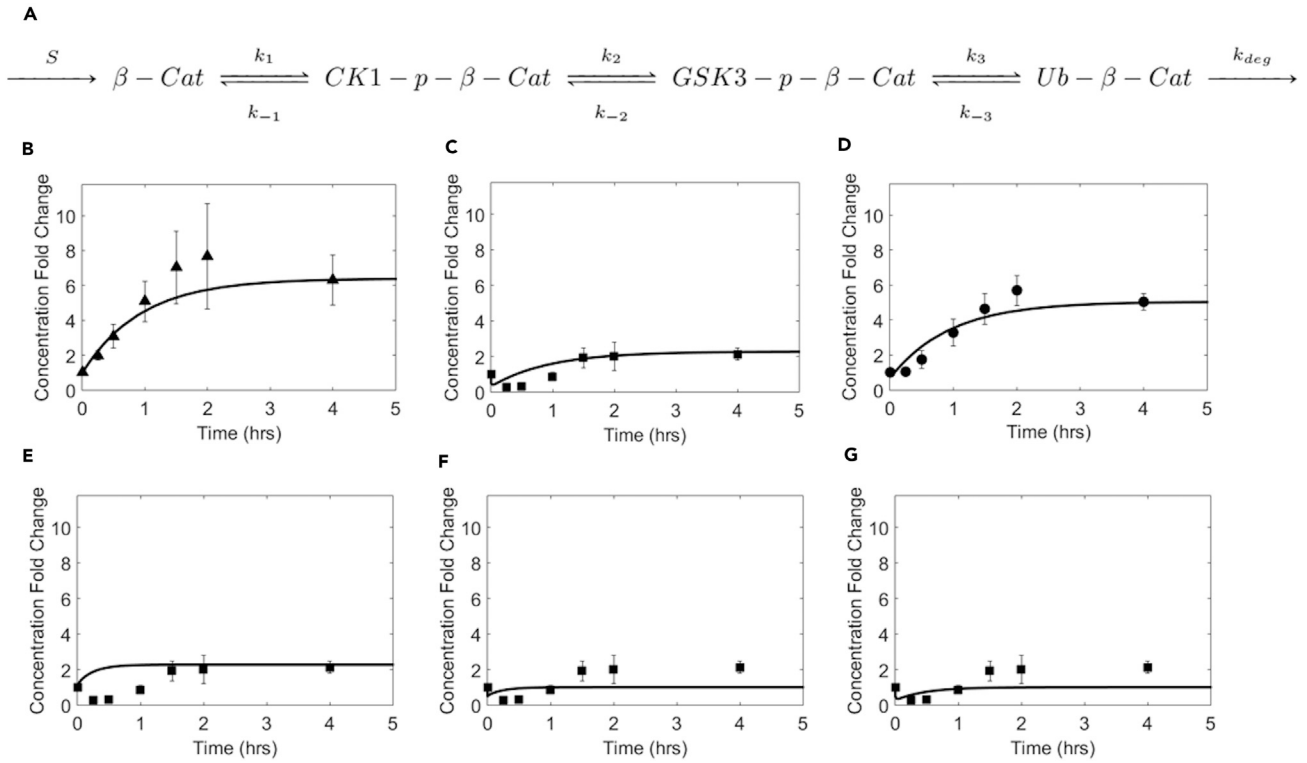


**Figure 3. Modeling β-Catenin Dynamics in Response to Wnt Stimulation**

(A) Cartoon showing sequential enzymatic modifications of β-catenin.

(B–D) Comparison of results from numerical integration of rate equations with experimental data for changes in concentrations of (B) total β-catenin, (C) GSK3-p-β-cat, and (D) CK1-p-β-cat. Values of the rate constants ($k_1$, $k_2$, and $k_3$) were each assumed to decrease to 0.44 times their original value, to reflect the decrease in the number of active destruction complexes.

(E–G) Comparison of results from numerical integration of rate equations with experimental data for changes in concentrations of GSK3-p-β-cat for a decrease in the value of (E) only $k_3$, (F) only $k_2$, and (G) $k_1$ and $k_2$, but not $k_3$. Experimental data in plots (B–G) show mean ±1 SD (n = 3 replicates).

See also Figure S3.

case, CK1-p-β-cat would remain bound to the destruction complex before its GSK3 phosphorylation, and the rate of GSK3 phosphorylation would be ($k_2$)[CK1-p-β-cat]; the rate constant for GSK3 phosphorylation, $k_2$ (Figure 3A), would then be independent of the destruction complex concentration and depend only on the intrinsic catalytic activity of GSK3 in the complex ($k_2 = k_{cat2}$). The concentration of CK1-p-β-cat at the new steady state should therefore return to its original value, so that the rate of GSK3 phosphorylation ($k_2$*[CK1-p-β-cat]) also recovers. In contrast, we see a significant (~5-fold) increase in the concentration of CK1-p-β-catenin upon Wnt stimulation (Figure 1D), similar to the significant increase in concentration of total β-catenin. This significant increase is inconsistent with a processive model and supports a distributive model for destruction complex activity, with the increase in CK1-p-β-cat concentration being necessary to compensate for the decrease in [DC]. CK1-p-β-cat would therefore be present in both free and destruction-complex-bound states.

As seen in Figure 1C, the concentration of GSK3-p-β-cat at the new steady state (following Wnt stimulation) is also greater than its initial value. Our co-immunoprecipitation results confirm that levels of destruction-complex-bound GSK3-p-β-cat recover to their original steady-state value upon Wnt stimulation. Collectively, these results suggest that GSK3-p-β-cat is also present in both free and destruction-complex-bound states. Moreover, these results are consistent with ubiquitination occurring primarily in an intact destruction complex as suggested by Li et al. (2012). An increase in the total concentration of GSK3-p-β-cat would be required if ubiquitination were occurring primarily in the destruction complex, to compensate for the decrease in the number of active destruction complexes upon Wnt stimulation. In contrast, if ubiquitination were occurring primarily outside the destruction complex, we would not expect to see an increase in total levels of GSK3-p-β-cat at the new steady state.

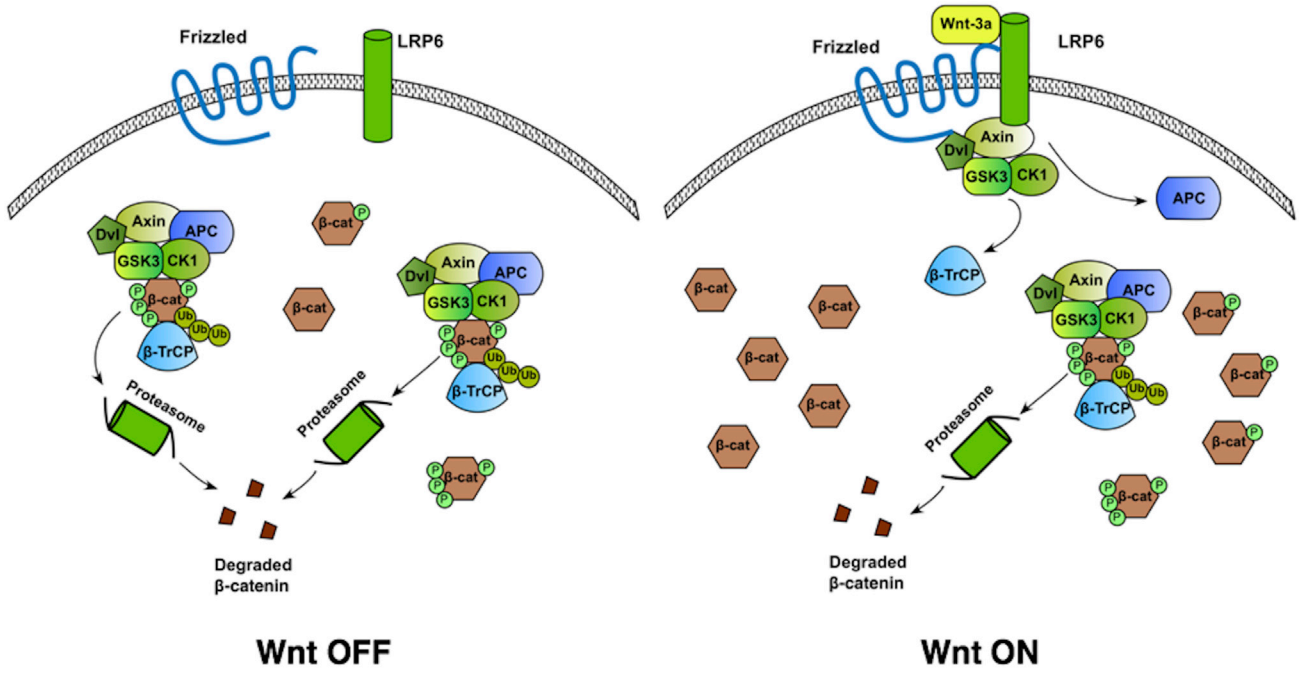


**Figure 4. Proposed Mechanism for Wnt Signaling**

(Left) In the absence of Wnt, all destruction complexes target cytosolic β-catenin for degradation. (Right) Wnt stimulation causes the disassembly of a fraction of the intracellular destruction complexes, inhibiting their ability to phosphorylate and ubiquitinate cytosolic β-catenin. Levels of free β-catenin increase until mass action results in a recovery of the rate of degradation of β-catenin by the active destruction complexes.

We used our results to predict β-catenin dynamics in response to Wnt signaling (Figures 3B–3D and Supplemental Information). In our proposed distributive model, the response to a Wnt signal is caused primarily by a decrease in the number of active destruction complexes, which causes a decrease in magnitudes of the rate constants for phosphorylation and ubiquitination—$k_1$, $k_2$, and $k_3$ (Figure 3A). The lines in Figures 3B–3D represent β-catenin concentrations obtained by numerical integration of the dynamical equations (see Supplemental Information, equations S1–S4) with the value of each of the rate constants $k_1$, $k_2$, and $k_3$ being decreased to 0.44 times their value before Wnt stimulation. The choice of 0.44 was guided by experimental data. The average Axin1/APC ratio upon Wnt stimulation ranged from ca. 0.39 to 0.5 times its value before Wnt stimulation (Figure 2D), and 0.44 lies in this range and is close to the average of these two values. As seen in Figures 3B–3D, the predicted changes in steady-state concentrations and the dynamical behaviors match the experimental results. In contrast, predictions based on inhibition of only ubiquitination (Figure 3E) or only phosphorylation (Figures 3F and 3G) do not explain the experimental results for β-catenin dynamics. If only ubiquitination is inhibited, results obtained by numerical integration of the dynamical equations do not show a dip in the concentration of GSK3-p-β-cat (Figure 3E). If only phosphorylation is inhibited, but not ubiquitination (Figures 3F and 3G), then GSK3-p-β-cat levels at the new steady state would recover to their initial value, but not exceed it, in contrast to experimental results. We note that whereas our experimental data are most consistent with a mechanism based on the inhibition of both phosphorylation and ubiquitination (Figures 3 and S3), our simulations do not perfectly match the experimental data for recovery of GSK3-p-β-cat concentrations. This difference could be due to factors not accounted for in our simple model. For instance, the inhibition could occur with a slight lag, and at different rates in different cells, due to heterogeneity in the time taken for Wnt to diffuse and bind to receptors on different cells and in the time required for complex disassembly.

In summation, our results support the following mechanistic model for Wnt signaling (Figure 4). Following Wnt stimulation, some of the destruction complexes relocate to the membrane, where they are associated with LRP6, and this subsequently leads to the dissociation of APC from the destruction complexes and the inhibition of GSK3 phosphorylation of β-catenin. The remaining destruction complexes remain intact and active in the cytoplasm. However, the initial decrease in the number of active destruction complexes results in an initial decrease in the rate of degradation of β-catenin. Consequently, free β-catenin is able to

accumulate, until mass action results in an increase in the levels of destruction-complex-bound GSK3-p-β-cat and a recovery of the rate of degradation of β-catenin, but at an elevated steady-state level of β-catenin. We note that although it is possible that there are also free kinases in the cell, numerous published reports have confirmed a primary role for destruction complexes in mediating β-catenin phosphorylation and degradation (Li et al., 2012). Destruction complex-mediated degradation of β-catenin may in fact facilitate the regulation of intracellular levels of β-catenin in response to external signals, allowing the binding of an "external" Wnt ligand to induce the relocation of destruction complexes to the membrane, their disassembly, and a resulting increase in levels of β-catenin. Recent reports have suggested a role for a spatially localized Wnt signal in asymmetric stem cell division (Habib et al., 2013). It is intriguing that the spatial patterning of destruction complex activity is itself central to the core Wnt signal transduction mechanism. Understanding this fundamental mechanism provides a rational basis for tuning the pathway for scientific and therapeutic purposes (Kahn, 2014; Nusse and Clevers, 2017).

## METHODS

All methods can be found in the accompanying Transparent Methods supplemental file.

## SUPPLEMENTAL INFORMATION

Supplemental Information includes Transparent Methods and three figures and can be found with this article online at https://doi.org/10.1016/j.isci.2018.07.007.

## ACKNOWLEDGMENTS

We acknowledge support from NIH grants R01 NS087253 and R01 NS083856.

## AUTHOR CONTRIBUTIONS

R.S.K., A.M., N.D., and D.V.S. designed experiments; A.M., N.D., and M.S. performed experiments and analyzed data; R.S.K. and A.M. wrote the manuscript with revision and editing from D.S., N.D., and M.S.

## DECLARATION OF INTERESTS

The authors declare no competing interests.

Received: April 12, 2018
Revised: June 22, 2018
Accepted: July 11, 2018
Published: August 31, 2018

## REFERENCES

Azzolin, L., Panciera, T., Soligo, S., Enzo, E., Bicciato, S., Dupont, S., Bresolin, S., Frasson, C., Basso, G., Guzzardo, V., et al. (2014). YAP/TAZ incorporation in the beta-catenin destruction complex orchestrates the Wnt response. Cell *158*, 157–170.

Bilic, J., Huang, Y.L., Davidson, G., Zimmermann, T., Cruciat, C.M., Bienz, M., and Niehrs, C. (2007). Wnt induces LRP6 signalosomes and promotes dishevelled-dependent LRP6 phosphorylation. Science *316*, 1619–1622.

Clevers, H. (2006). Wnt/beta-catenin signaling in development and disease. Cell *127*, 469–480.

Cong, F., Schweizer, L., and Varmus, H. (2004). Wnt signals across the plasma membrane to activate the beta-catenin pathway by forming oligomers containing its receptors, frizzled and LRP. Development *131*, 5103–5115.

Debets, M.F., van Berkel, S.S., Schoffelen, S., Rutjes, F., van Hest, J.C.M., and van Delft, F.L. (2010). Aza-dibenzocyclooctynes for fast and efficient enzyme PEGylation via copper-free (3+2) cycloaddition. Chem. Commun. *46*, 97–99.

Dieterich, D.C., Lee, J.J., Link, A.J., Graumann, J., Tirrell, D.A., and Schuman, E.M. (2007). Labeling, detection and identification of newly synthesized proteomes with bioorthogonal non-canonical amino-acid tagging. Nat. Protoc. *2*, 532–540.

Habib, S.J., Chen, B.C., Tsai, F.C., Anastassiadis, K., Meyer, T., Betzig, E., and Nusse, R. (2013). A localized Wnt signal orients asymmetric stem cell division in vitro. Science *339*, 1445–1448.

Hendriksen, J., Jansen, M., Brown, C.M., van der Velde, H., van Ham, M., Galjart, N., Offerhaus, G.J., Fagotto, F., and Fornerod, M. (2008). Plasma membrane recruitment of dephosphorylated beta-catenin upon activation of the Wnt pathway. J. Cell Sci. *121*, 1793–1802.

Hernandez, A.R., Klein, A.M., and Kirschner, M.W. (2012). Kinetic responses of beta-catenin specify the sites of Wnt control. Science *338*, 1337–1340.

Kahn, M. (2014). Can we safely target the WNT pathway? Nat. Rev. Drug Discov. *13*, 513–532.

Kim, S.E., Huang, H., Zhao, M., Zhang, X., Zhang, A., Semonov, M.V., MacDonald, B.T., Zhang, X., Garcia Abreu, J., Peng, L., and He, X. (2013). Wnt stabilization of beta-catenin reveals principles for morphogen receptor-scaffold assemblies. Science *340*, 867–870.

Kitazawa, M., Hatta, T., Ogawa, K., Fukuda, E., Goshima, N., and Natsume, T. (2017). Determination of rate-limiting factor for formation of beta-catenin destruction complexes using absolute protein quantification. J. Proteome Res. *16*, 3576–3584.

Li, V.S., Ng, S.S., Boersema, P.J., Low, T.Y., Karthaus, W.R., Gerlach, J.P., Mohammed, S., Heck, A.J., Maurice, M.M., Mahmoudi, T., and Clevers, H. (2012). Wnt signaling through inhibition of beta-catenin

degradation in an intact Axin1 complex. Cell *149*, 1245–1256.

Nelson, W.J., and Nusse, R. (2004). Convergence of Wnt, beta-catenin, and cadherin pathways. Science *303*, 1483–1487.

Nusse, R., and Clevers, H. (2017). Wnt/beta-catenin signaling, disease, and emerging therapeutic modalities. Cell *169*, 985–999.

Nusse, R., and Varmus, H. (2012). Three decades of Wnts: a personal perspective on how a scientific field developed. EMBO J. *31*, 2670–2684.

Peifer, M., and Polakis, P. (2000). Wnt signaling in oncogenesis and embryogenesis–a look outside the nucleus. Science *287*, 1606–1609.

Tan, C.W., Gardiner, B.S., Hirokawa, Y., Layton, M.J., Smith, D.W., and Burgess, A.W. (2012). Wnt signalling pathway parameters for mammalian cells. PLoS One *7*, e31882.

Valvezan, A.J., Zhang, F., Diehl, J.A., and Klein, P.S. (2012). Adenomatous polyposis coli (APC) regulates multiple signaling pathways by enhancing glycogen synthase kinase-3 (GSK-3) activity. J. Biol. Chem. *287*, 3823–3832.

ISCI, Volume *6*

## Supplemental Information

# Understanding How Wnt Influences Destruction Complex Activity and β-Catenin Dynamics

**Abhirup Mukherjee, Neha Dhar, Mark Stathos, David V. Schaffer, and Ravi S. Kane**

**Supplementary Information:**

**Transparent Methods:**

**Mammalian Cell Culture and treatment with Wnt-3A and MG132**

Human embryonic kidney (HEK293T) cells were purchased from the American Type Culture Collection (ATCC CRL-11268) and cultured in Dulbecco's Modified Eagle Medium (High-glucose DMEM; Gibco 11995065) supplemented with 10% HI-FBS (Heat-Inactivated Fetal Bovine Serum; Gibco 10438018) and 1% penicillin-streptomycin (Gibco) (hereon referred to as D-10 media) in a humidified incubator at 37°C with 5% $CO_2$. Cultured mammalian cells were treated with recombinant human Wnt-3A (R&D Systems; 5036-WN) at a final concentration of 750-1000 ng/ml for the indicated time periods. Proteasomal inhibitor MG132 (Sigma-Aldrich; M7449) treatment was done at a working concentration of 20 μM for the time periods mentioned in the article.

**Antibodies**

The following antibodies were used for immunoblotting and immunoprecipitation; anti-β-catenin (BD Transduction Laboratories; #610153), anti-phospho-β-catenin antibody (Ser33/37/Thr41) (Cell Signaling Technology; #9561), anti-phospho-β-catenin antibody (Ser45) (Cell Signaling Technology; #9564), anti-APC (Cell signaling Technology, #2504), anti-APC (Abcam; #ab15270), anti-Axin1 (Cell Signaling Technology; #2087), monoclonal rabbit IgG isotype control (Abcam; #ab172730), anti-LRP6 (C5C7) antibody (Cell Signaling Technology; #2560), anti-α-tubulin (Abcam; #ab52866), anti-Histone H3 (Abcam; #ab1791), anti-biotin (Abcam; #ab53494) and anti-GAPDH (Abcam; #ab8245).

**Harvesting cells and preparation of whole-cell lysates and cytoplasmic and nuclear extracts for time series experiments**

HEK293T cells were cultured in 6-well tissue culture plates (Corning) at an initial concentration of 1.5 million cells per well and allowed to grow 80-90% confluent after approximately 36-48 h. After experimentation, the cells were washed in ice-cold DPBS (Corning) twice and lysed in a lysis buffer of DPBS containing 0.5% digitonin (pH 7.5) (Kim *et al.*). The cells were incubated on ice for 30-45 min for complete lysis and then harvested using cell scrapers. The residual debris in the lysate was spun down after centrifugation at 13,000 g for 15 min. The supernatant was used as the whole-cell lysate for further analysis.

To obtain the cytoplasmic and nuclear extract of HEK293T cells, the above supernatant was incubated with Concanavalin A-Sepharose 4B (GE Healthcare) beads for 60 min at 4°C. After incubation, the beads were spun down at 3000g for 5 mins. The cytoplasmic and nuclear fractions of the lysates were in the supernatant and the membrane-associated proteins were bound to the Concanavalin A beads. The whole-cell lysates and cytoplasmic and nuclear fractions of the lysates were denatured after the addition of LDS Sampling Buffer (Thermo Scientific) at 100°C for 10-15 mins and then processed for immunoblotting (western blots).

**BONCAT and detection of newly synthesized protein**

Methionine-free, cystine-free Dulbecco's Modified Eagle Medium (DMEM) containing 4 mM of L-Azidohomoalanine or L-AHA (Anaspec; #AS-63669) was used for the unnatural amino acid tagging experiments. HEK293T cells were cultured in 15 cm tissue culture dishes (Corning) at an initial concentration of 15 million cells per dish for 36-48 hours in D-10 media. After the cells were treated with Wnt-3A for 0.5 hours, the D-10 media was removed and the cells were washed twice with DPBS followed by one wash with methionine-free, cystine-free Dulbecco's Modified

Eagle Medium (DMEM). The cells then treated with L-AHA containing DMEM (containing 20 μM MG-132 and Wnt-3A as mentioned in the article) for 2.5 hours. The cells were then washed twice with ice-cold DPBS (Corning) and lysed using 2% SDS in DPBS containing phosphatase (Sigma-Aldrich) and protease inhibitor (Thermo Scientific) cocktails at concentrations prescribed by the manufacturer(s). The lysates were subsequently denatured by boiling at 100°C for 15 mins. To reduce the viscosity of the protein lysates, the samples were treated with benzonase nuclease (Sigma Aldrich; #E1014) at 37°C for 30 mins with constant mixing. 10 mg of total processed lysates were reacted with 150 μM DBCO-sulfo-biotin for 3-5 hours at room temperature. The reaction was quenched with excess L-AHA and passed through PD-10 (GE Healthcare) desalting columns to remove unreacted DBCO-sulfo-biotin and other low molecular weight compounds. The biotin-tagged proteins were then quantified using a semi-quantitative dot-blot (as per Dieterich *et al.*). The biotin-tagged proteins were finally extracted by incubating with Streptavidin-agarose beads (Thermo Scientific) for 2 hours at room temperature. Streptavidin beads were then washed with 2% SDS in PBS 5-6 times to remove the non-biotin tagged proteins. The protein mixture was then denatured using the LDS Sample Loading Buffer (Thermo Scientific) at 100°C for 10-15 min and loaded onto 4-12% Bis-Tris Gels for further analysis.

**Co-Immunoprecipitation (Co-IP)**

HEK293T cells were cultured in 15-cm tissue culture dishes (Corning) at an initial concentration of 15 million cells per dish and incubated in D-10 media for approximately 36-48 hours till 80% confluency. After experimentation, the cells were washed in ice-cold DPBS (Corning) twice and lysed in ~2 ml of lysis buffer containing 25 mM Tris-HCl pH 7.4, 150 mM NaCl, 1% NP-40, 1 mM EDTA, 5% glycerol (for anti-APC IP) or 150 mM NaCl, 30 mM Tris (pH 7.5), 1 mM EDTA, 1% Triton X-100, 10% Glycerol (for anti-Axin1 IP). Lysis buffers were supplemented

with 0.1 mM PMSF, 0.5 mM DTT, phosphatase inhibitor cocktails 2 &3 (at 1:100 dilution) (Sigma) and Halt protease inhibitor cocktail (at 1:100 dilution) (Thermo Scientific). The cells were then incubated on ice for 30-45 mins, harvested and spun down at speeds mentioned earlier. After being spun down at 13,000 g for 15 mins, cell lysates were pre-cleared by incubating with Rabbit IgG isotype control antibody (Abcam, #ab172730) for 4 hours followed by Pierce Protein A Magnetic beads (Thermo Scientific) for 2 hours at 4°C. A magnetic rack (MagnaRack; Thermo Scientific) was then used to separate out the magnetic beads and the supernatant was then incubated overnight with the appropriate antibody at 4°C with constant mixing. The lysate was then incubated in Protein A magnetic beads for 2 hours at 4°C with constant mixing. The magnetic beads were then separated using the MagnaRack, washed 5 times with TBS containing 0.1% Tween-20 and then by 1x TBS. The beads were then denatured in 2x LDS Sampling Buffer with 2-mercaptoethanol by heating at 95-100°C for 15 mins. The magnetic beads were again separated and the supernatant containing the immunoprecipitated proteins were analyzed using immunoblotting.

**SDS-PAGE Gel Electrophoresis and Immunoblotting**

Proteins in the lysates were resolved using SDS-PAGE in 3-8% Tris-Acetate (for detecting APC) and 4-12% Bis-Tris Polyacrylamide gels (for all other proteins) in OWL P8DS (Thermo Scientific). The proteins were then transferred to a nitrocellulose membrane using electrophoretic transfer in the Trans-Blot Turbo Transfer System (Bio-Rad).

For immunoblotting, the membrane was blocked in a blocking buffer (TBS, 0.1% Tween-20, 5% non-fat dry milk or BSA; per antibody manufacturer's recommendation) for 1 hour at room temperature. The membrane was then incubated overnight at 4°C in primary antibody diluted in 5% BSA in TBST (TBS, 0.1% Tween-20). The dilution used for different antibodies was

optimized for individual applications, using the manufacturer's recommendation as the starting point. After the primary antibody incubation, the membrane was washed three times with TBST for 5 min each and then incubated in secondary antibody diluted in the blocking buffer for 1 hour at room temperature. For total β-catenin detection, an HRP-conjugated anti-mouse antibody (Jackson Immunoresearch) was used at a dilution of 1:10000. In all other cases, an HRP-conjugated anti-rabbit antibody (Thermo Scientific) was used at a dilution of 1:3000-1:5000. The protein bands in the membrane were then detected in a ChemiDoc MP Imaging system (Bio-Rad) using the SuperSignal West Femto Maximum Sensitivity Substrate. Quantitation of the protein concentration from the detected protein bands was carried out by using the analysis tools provided in the Image Lab Software (Bio-Rad) and validated using the ImageJ software in the previously ascertained linear dynamic range of concentrations for respective proteins.

**Modeling β-catenin dynamics**

$B_0$, $B_1$, $B_2$, and $B_3$ represent unphosphorylated β-catenin, CK1-phosphorylated β-catenin, GSK3-phosphorylated β-catenin, and ubiquitylated β-catenin, respectively(Hernandez et al., 2012) respectively. S represent the rate of synthesis of β-catenin, $[B_i]$ denote concentrations (i = 0, 1, 2, 3), and $k_{deg}$ and $k_{j,}$ (j = ±1, ±2, ±3) denote rate constants. The phosphorylation and degradation of β-catenin is modeled using the following dynamical equations (Hernandez et al., 2012):

$$\frac{d[B_0]}{dt} = S - k_1[B_0] + k_{-1}[B_1] \quad \text{(S1)}$$

$$\frac{d[B_1]}{dt} = k_1[B_0] - (k_2 + k_{-1})[B_1] + k_{-2}[B_2] \quad \text{(S2)}$$

$$\frac{d[B_2]}{dt} = k_2[B_1] - (k_3 + k_{-2})[B_2] + k_{-3}[B_3] \quad \text{(S3)}$$

$$\frac{d[B_3]}{dt} = k_3 B_2 - (k_{deg} + k_{-3})[B_3] \quad \text{(S4)}$$

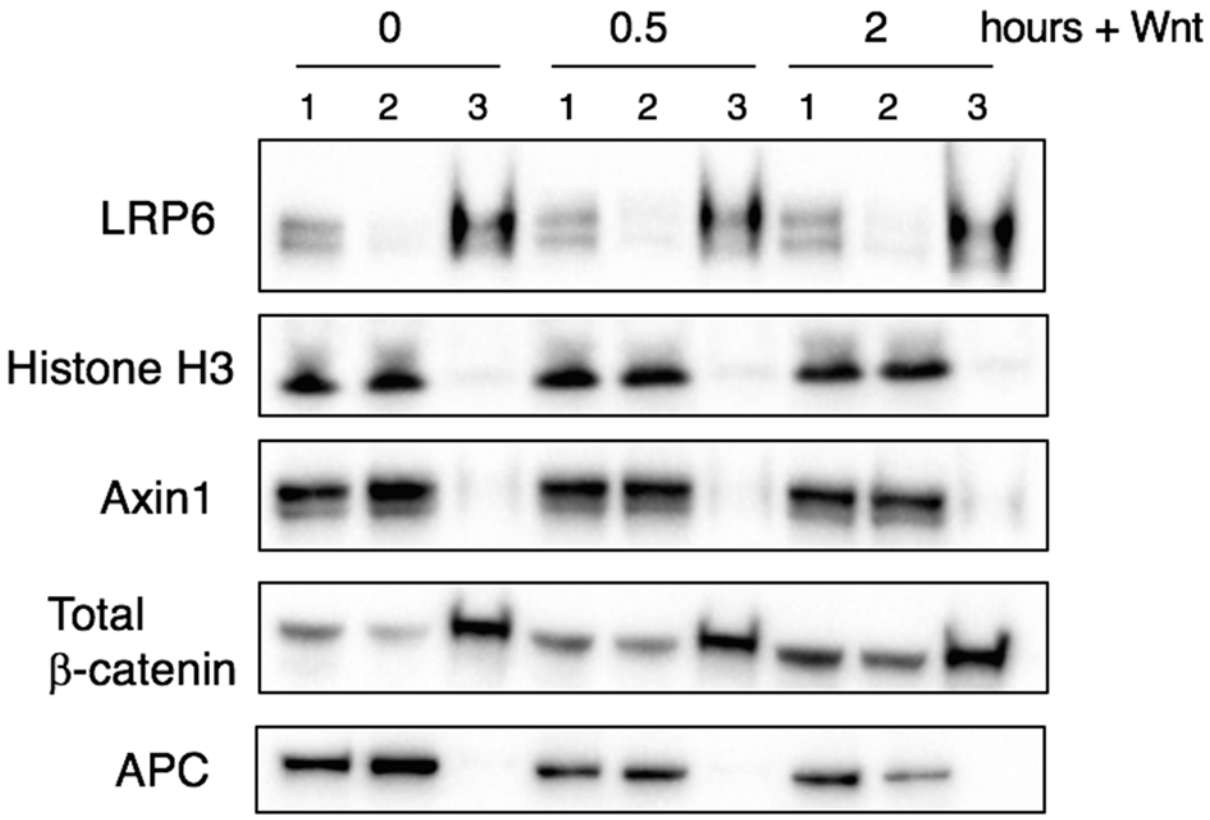


**Figure S1, related to Fig. 1. Characterization of protein fractions after pull-down using Concanavalin A-Sepharose 4B beads at different time points following Wnt-3A stimulation.** Within each time point, Lane 1 shows the protein in whole cell lysates, Lane 2 shows the flow-through after treatment with Concanavalin A-Sepharose 4B beads, and Lane 3 shows proteins eluted from the beads.

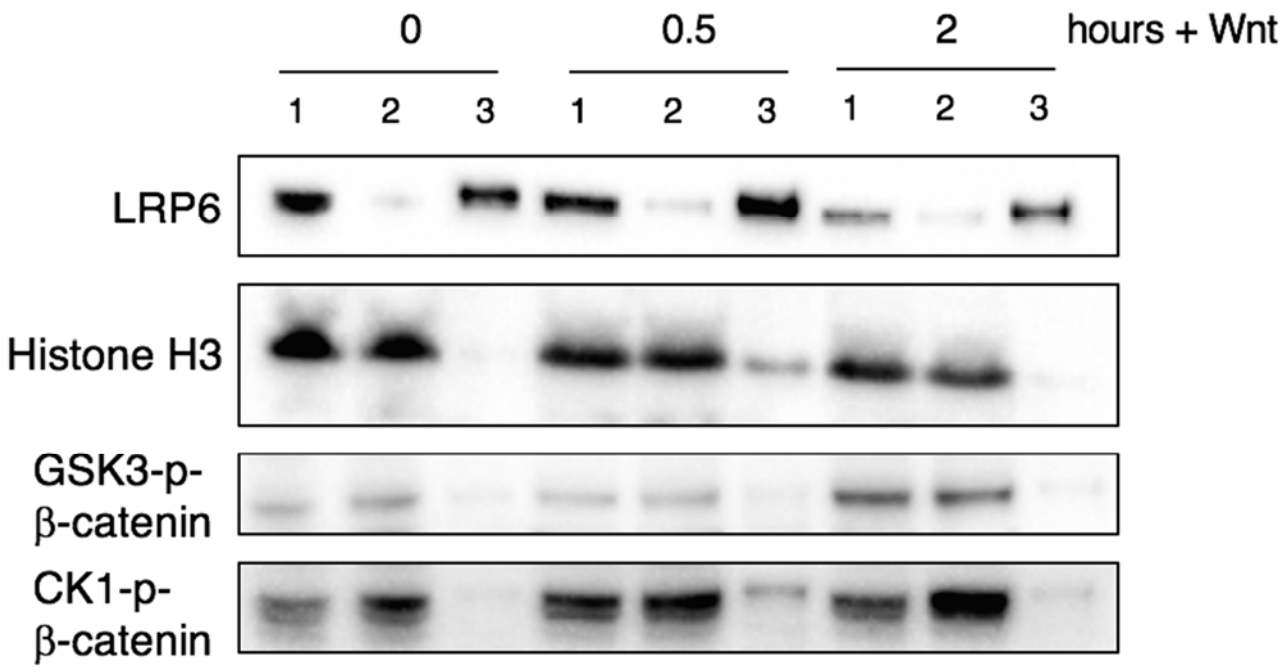


**Figure S2, related to Fig. 2. Characterization of protein fractions after pull-down using Concanavalin A-Sepharose 4B beads at different time points following Wnt-3A stimulation.** Within each time point, Lane 1 shows the protein in whole cell lysates, Lane 2 shows the flow-through after treatment with Concanavalin A-Sepharose 4B beads, and Lane 3 shows proteins eluted from the beads.

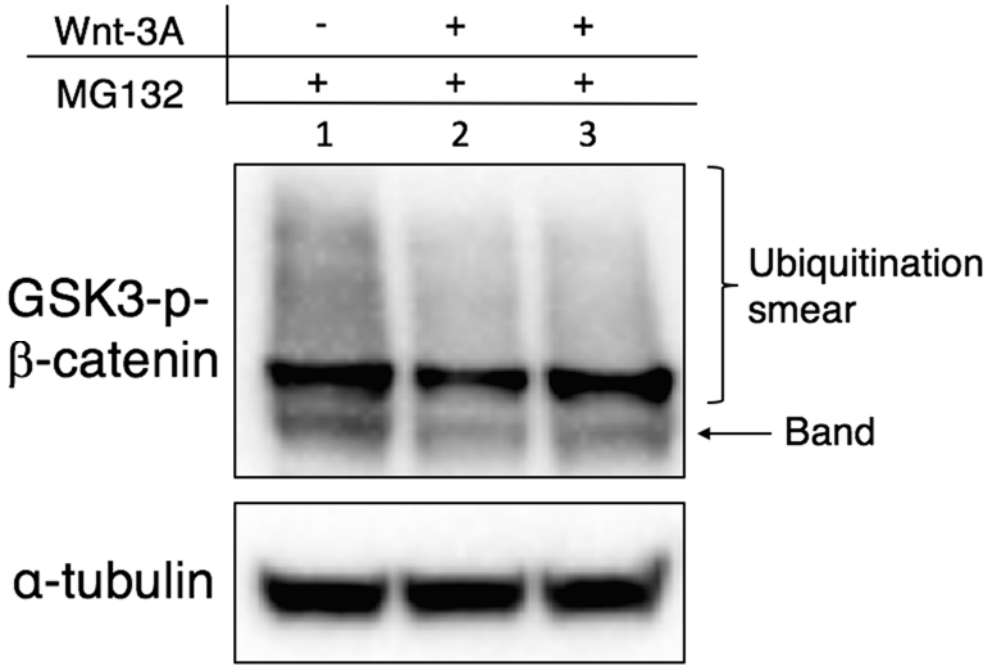


**Figure S3, related to Fig. 3. Ubiquitinated GSK3-p-β-catenin levels in presence of Wnt signaling.** Lane 1 and Lane 2 shows ubiquitinated GSK3-p-β-catenin levels in absence and presence of Wnt-3A respectively. The protein loading in Lane 3 was adjusted to compare ubiquitination levels for the same amount of GSK3-p-β-catenin in absence and presence of Wnt-3A respectively.